Residual energy in plasmas produced by intense subpicosecond lasers

B. M. Penetrante and J. N. Bardsley
High Temperature Physics Division, Lawrence Livermore National Laboratory, Livermore, California 94550
(Received 20 December 1989; revised manuscript received 5 November 1990)

This paper presents parameter studies to find the optimum conditions for the production of a cold highly ionized plasma suitable for the generation of recombination x-ray lasers. The effect of space-charge fields on the residual electron energy of optical-field-ionized plasmas is studied using a classical theory of above-threshold ionization and particle-in-cell simulations. The dependence of the residual energy on the pump-laser wavelength and peak intensity is strongly influenced by the dependence of the quiver energy on these parameters. The effect of space-charge fields indicates that the residual energy can be minimized by a suitable matching of the laser pulse length to the plasma density. The effect of collisional heating on the residual energy is also discussed.

I. INTRODUCTION

There are two ways of implementing the recombination scheme to produce x-ray lasing in optical-field-ionized plasmas. The "traditional" approach involves conditions in which the temperature of the plasma is rapidly decreased.[1–7] Cooling is achieved either by rapid expansion[5] or by radiative cooling.[7] The gain increases as the plasma cools, and peaks well after the pump laser is over. The population inversions are produced between excited states of the recombining ions. The time scale for the gain duration is thus of the order of a recombination time, and is referred to as the quasi-steady-state regime. X-ray lasing has been reported from laser-produced plasmas using these rapid cooling techniques.[7–9]

The other approach involves optical-field-ionized plasmas consisting of fully stripped ions (or heliumlike ions) and cold electrons.[2,10] Immediately after the pump laser pulse, inversion occurs in hydrogenlike ions (or lithiumlike ions) during the initial cascade of population through the excited levels of the ion. The gain duration is of the order of the radiative lifetime of the lasing transition, which is short compared with the recombination time, and is referred to as the transient regime. X-ray lasing using this approach has not been implemented to date. However, recent advances in high-intensity ultrashort-pulse lasers make this approach feasible. The major advantage of short-pulse laser-pumped x-ray lasers is their ability to access very short-wavelength resonance lines with high efficiency at achievable pump intensities. Moreover, this approach provides an ideal way of preparing the target medium for producing gain later in time on the type of transitions encountered in rapidly cooled recombination lasers.

There are two conditions that must be satisfied in order to produce gain using ultrashort-pulse lasers. The first condition is that the target media must be ionized to the fully stripped state (or to the heliumlike state to implement lithiumlike recombination schemes). Short-pulse low-frequency lasers with intensities of over 10^{16} W/cm^2 have been demonstrated clearly and equipment designed to produce 10^{18}–10^{21} W/cm^2 is under construction in several laboratories.[11–20] Laser intensities around 10^{17} W/cm^2 are sufficient to produce fully stripped lithium ions or heliumlike neon ions.

The second condition that must be satisfied is that the residual electron energy produced immediately after the pump laser pulse must be low enough so that the system is far from ionization equilibrium and strong three-body recombination commences immediately. This condition can be achieved if the electrons can be persuaded to return most of their quiver energy to the laser field.[2,10] Analysis of the dynamics of single electrons in plane-wave electromagnetic fields suggest that this may be possible using linearly polarized light, provided the electrons produced during the ionization process have low energies and interact only with the plane-wave radiation.[21,22]

Field-induced ionization produces a distribution of surplus electron energy in excess of that due to the coherent oscillation of the free electron in the electromagnetic field. This excess electron energy has been observed experimentally and has come to be known as above-threshold ionization (ATI).[23–26] In the regime of interest to recombination x-ray lasing, the electron quiver energy is much greater than the ionization potential and the photon energy of the pumping laser. In this regime ATI can be understood from classical considerations.[10,25,26] Classically, the excess electron energy can be attributed to the mismatch between the phase at the instant of ionization and the crest of the electromagnetic wave.[10] For linearly polarized light the ionization occurs predominantly at those parts of the optical cycle in which the field has its greatest magnitude, and the average ATI energy is small. Thus the ATI energy may be kept well below the ionization potential of the ion in question.

In addition to the ATI energy, there are other factors that could contribute to the residual electron energy. These are (i) plasma oscillations, (ii) elastic electron-ion collisions, and (iii) spatial inhomogeneities in the laser field. The first factor is significant if the space-charge forces are not too strong. Plasma oscillations can result from the ponderomotive expulsion of the electrons during the laser pulse. After the pulse the space-charge force between these electrons and the "stationary" ions causes

these electrons to rush back in. The electrons oscillate as the total energy flips between the space-charge field energy and the kinetic energy. This energy is eventually converted to thermal energy by collisions.

The second factor could become significant for long pulses. Collisional heating associated with elastic electron-ion collisions could increase the residual energy by transferring energy from ordered quiver motion to random motion. This is known as strong-field inverse bremsstrahlung.

The third factor becomes significant for tightly focused laser beams. The ponderomotive expulsion of the electrons could cause some electrons to leave the laser focus. These electrons acquire an energy equal to the ponderomotive potential. This is known as ponderomotive heating. In the literature ATI often includes contributions from this effect.

The purpose of this paper is to provide a systematic study of the contributions of the various heating processes to the residual electron energy. We study the sensitivity of the residual electron energy to the system parameters. These parameters are the ion density, laser-pulse length, wavelength, intensity, and spot size. It has been previously suggested that in order to keep the residual electron energy small, the electrons must interact with the electromagnetic field in a nearly adiabatic fashion as the laser pulse passes. However, the consequent limits on the pulse length have not been established. It has also not been determined quantitatively how much effect the space-charge field has on the interaction between the electrons and the laser field.

The calculation of the ATI energy is dependent on the ionization rate. In highly intense fields light atoms will be completely stripped and heavy atoms will lose most of their electrons. The natural frequencies of the remaining electrons are very high compared with the frequency of the lasers in current use, so the high-field ionization rates depend very weakly on the laser frequency and can be estimated from dc tunneling rates. In Sec. II we compare various models[27–31] of high-field ionization in order to indicate the sensitivity of the ATI energy on the rate formula. In Sec. III the classical theory of ATI is used to show how the residual electron energy depends on the laser wavelength, peak intensity, spot size, and pulse length.

Even if plasma oscillations are not established the space-charge forces could modify the ATI energy. When there are substantial space-charge forces the points, in time and space, at which the electron energy is minimum do not correspond to the points where the laser field is maximum. Thus there is no reason to expect that the electrons created near the crest of the electromagnetic wave will return most of their quiver energy to the field.[22] In Sec. IV we study how the presence of a space-charge field affects the ATI energy. It is shown that by properly matching the laser-pulse length to the strength of the space-charge force, the residual energy can be reduced significantly.

Computer simulations of the effects of space-charge forces on the electron dynamics are given in Sec. V. The inclusion of the laser ionization process in the simulation provides for an initial plasma profile and ionization levels which are consistent with the prescribed laser pulse. The simulations employ a particle-in-cell code in which the space-charge forces are calculated consistently from the spatial distribution of the charges.[32–35] The residual electron energy is presented as a function of the gas density, laser wavelength, pulse length, and spot size. It is shown that there are two resonant regions that produce large residual electron energies. One is where the plasma period is close to the laser oscillation period; the other is where the plasma period is close to the pulse length. In the high-density region in which the plasma oscillations are suppressed, it is shown that the residual energy varies approximately as the cube of the laser wavelength, and is independent of the spot size. The results of the simulation are consistent with the classical theory of ATI in the presence of space-charge forces. The effect of collisional heating is discussed in Sec. VI.

II. PHOTOIONIZATION IN VERY STRONG FIELDS

The lasers currently being used for short-pulse experiments range from neodynium glass lasers, with $\lambda=1$ μm and $\hbar\omega=1.2$ eV to excimer lasers such as KrF, with $\lambda=0.25$ μm and $\hbar\omega=5$ eV. For laser intensities above 10^{16} W/cm^2, light atoms will be completely stripped and heavy atoms will lose many electrons. The electrons that remain bound as the laser intensity rises to its maximum value have high ionization potentials and high natural frequencies compared with that of the driving laser. To the ions that are found in the focal region near the center of the laser pulse, the laser frequency appears to be very low. Thus the high-field ionization rates depend very weakly on frequency and can be computed from dc tunneling rates.[29]

The level of ionization reached during the laser pulse can be estimated using a simple Coulomb-barrier model. The threshold intensity for the production of charge state Z through the ionization of an electron with effective principal quantum number $n_{\rm eff}$ can be found by examining the combined potential formed by the Coulomb potential and the external electric field. If the field depression of the potential barrier exceeds the binding energy of the electron, ionization will occur rapidly. If the Stark-shift level is ignored, the resulting field strength is

$$E_{\rm th}=\frac{Z^3}{16n_{\rm eff}^4}E_{\rm a.u.}\ ,$$

where $E_{\rm a.u.}$ is the atomic field strength (5.1×10^9 V/cm). The effective quantum number is obtained by equating the ionization potential U_i of the critical electron orbit with $(Z^2/n_{\rm eff}^2)U_{\rm H}$,

$$n_{\rm eff}=\frac{Z}{(U_i/U_{\rm H})^{1/2}}\ ,$$

where $U_{\rm H}$ is the ionization potential of hydrogen ($=13.6$ eV) and Z refers to the residual charge seen by this electron. Allowance for the Stark shift increases the threshold field by a factor of approximately 50%. This leads to a threshold intensity

$$I_{\rm th}=\frac{2.2\times10^{15}}{Z^2}\left[\frac{U_i}{27.21}\right]^4 \ {\rm W/cm^2} \ . \tag{1}$$

Experiments by Augst *et al.*[31] have shown that for a laser wavelength of 1 μm and pulse length of 1 ps, the ionization of noble gases can be accurately described by this dc tunneling model. One of the important features observed in the experiments by Augst *et al.* is the dependence of the threshold laser intensity on both the ionization potential and the charge state of the species.

Figure 1 shows the laser intensity required to produce various ions that are of interest to x-ray lasing. The associated x-ray laser wavelengths corresponding to each ion are also shown. Intensities as low as 10^{16} W/cm^2 are sufficient to produce lasing in helium or nitrogen, while intensities between 10^{18} and 10^{19} W/cm^2 are required to produce lasing at 33 Å in carbon. The threshold intensities shown in Fig. 1 are close to those calculated by Burnett and Corkum,[10] who used the ionization rate formula for hydrogenlike ions.[29] In their calculation the required laser intensities were obtained by requiring an ionization rate of 10^{12} s^{-1}.

The Keldysh formula[27] for the ionization rate is commonly used to describe high-intensity laser-atom interactions. An important feature of the Keldysh theory is that the ionization rate is determined more by the properties of the outgoing electron than by the details of the atomic structure. The full form of the Keldysh formula for the ionization rate is

$$W=A\omega\left[\frac{U_i(0)}{\hbar\omega}\right]^{3/2}\left[\frac{\gamma}{(1+\gamma^2)^{1/2}}\right]^{5/2}S\left[\gamma,\frac{U_i(\omega)}{\hbar\omega}\right]$$

$$\times\exp\left[-\frac{2U_i(\omega)}{\hbar\omega}\left[\sinh^{-1}\gamma-\gamma\frac{(1+\gamma^2)^{1/2}}{1+2\gamma^2}\right]\right], \tag{2}$$

where γ is the tunneling parameter given by

$$\gamma=\omega\frac{\sqrt{2mU_i(0)}}{eE} \ ,$$

E is the electric field strength, ω is the laser frequency, and $U_i(0)$ is the field-free ionization potential. The other terms in the formula are

$$U_i(\omega)=U_i(0)\left[1+\frac{1}{2\gamma^2}\right] \ ,$$

$$S\left[\gamma,\frac{U_i(\omega)}{\hbar\omega}\right]=\sum_{m=0}^{\infty}\left\{\exp\left[-\left[2\left\langle\frac{U_i(\omega)}{\hbar\omega}+1\right\rangle-\frac{U_i(\omega)}{\hbar\omega}+m\right]\left[\sinh^{-1}\gamma-\frac{\gamma}{(1+\gamma^2)^{1/2}}\right]\right]\right\}$$

$$\times\Phi\left\{\left[\frac{2\gamma}{(1+\gamma^2)^{1/2}}\left[\left\langle\frac{U_i(\omega)}{\hbar\omega}+1\right\rangle-\frac{U_i(\omega)}{\hbar\omega}+m\right]\right]^{1/2}\right\} \ ,$$

$$\Phi(x)=\int_0^x\exp(t^2-x^2)dt \ .$$

The factor A in Eq. (2) is of order unity and accounts for a weak dependence upon the details of the atom.

The tunneling ionization theory of Ammosov, Delone, and Krainov[30] is also commonly used to describe laser-atom interactions in strong fields. The ionization rate is given by

$$W=1.61\omega_{\rm a.u.}\frac{Z^2}{n_{\rm eff}^{4.5}}\left[10.87\frac{Z^3}{n_{\rm eff}^4}\frac{E_{\rm a.u.}}{E}\right]^{2n_{\rm eff}-1.5}$$

$$\times\exp\left[-\frac{2}{3}\frac{Z^3}{n_{\rm eff}^3}\frac{E_{\rm a.u.}}{E}\right], \tag{3}$$

where $\omega_{\rm a.u.}$ is the atomic unit of frequency ($=4.1\times10^{16}$ s^{-1}). It has been pointed out by Ammosov *et al.*[30] that Eq. (3) agrees well with experimental data[36] on tunnel ionization (using a 1-ns, 10-μm laser) of atoms and atomic ions of noble gases.

Figure 2 shows the ionization rates for neon as calculated using the full Keldysh formula and the Ammosov *et al.* formula. The Keldysh ionization rates are weakly dependent on the laser wavelength for the low charge states. The dependence on wavelength grows stronger at the higher charge states. The Ammosov *et al.* ionization rates are much larger than the Keldysh rates. Experiments by Perry *et al.*[37] (using a 1-ps, 0.586-μm laser with intensities of 10^{13}–5×10^{14} W/cm^2) show that the Keldysh theory is good only for the production of the first

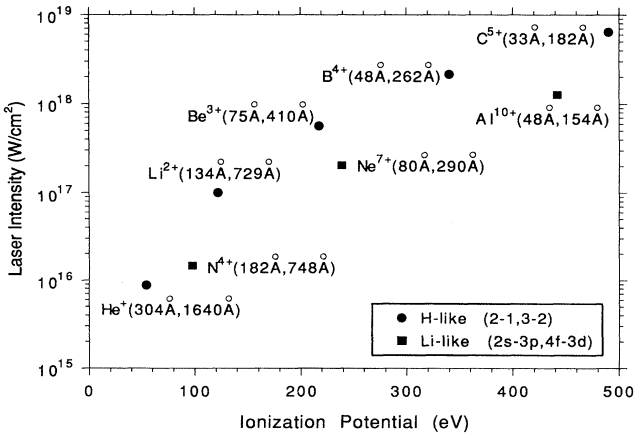

FIG. 1. Laser intensity [calculated using Eq. (1)] required to produce various ions of interest to recombination x-ray lasing. The candidate x-ray laser wavelengths are also shown.

charge state. Later experiments by Augst *et al.*[31] (using a 1-ps, 1-μm laser with intensities of $10^{14}-5\times10^{16}$ W/cm^2) confirm that the Ammosov *et al.* rates are in better agreement with the data than the Keldysh rates.

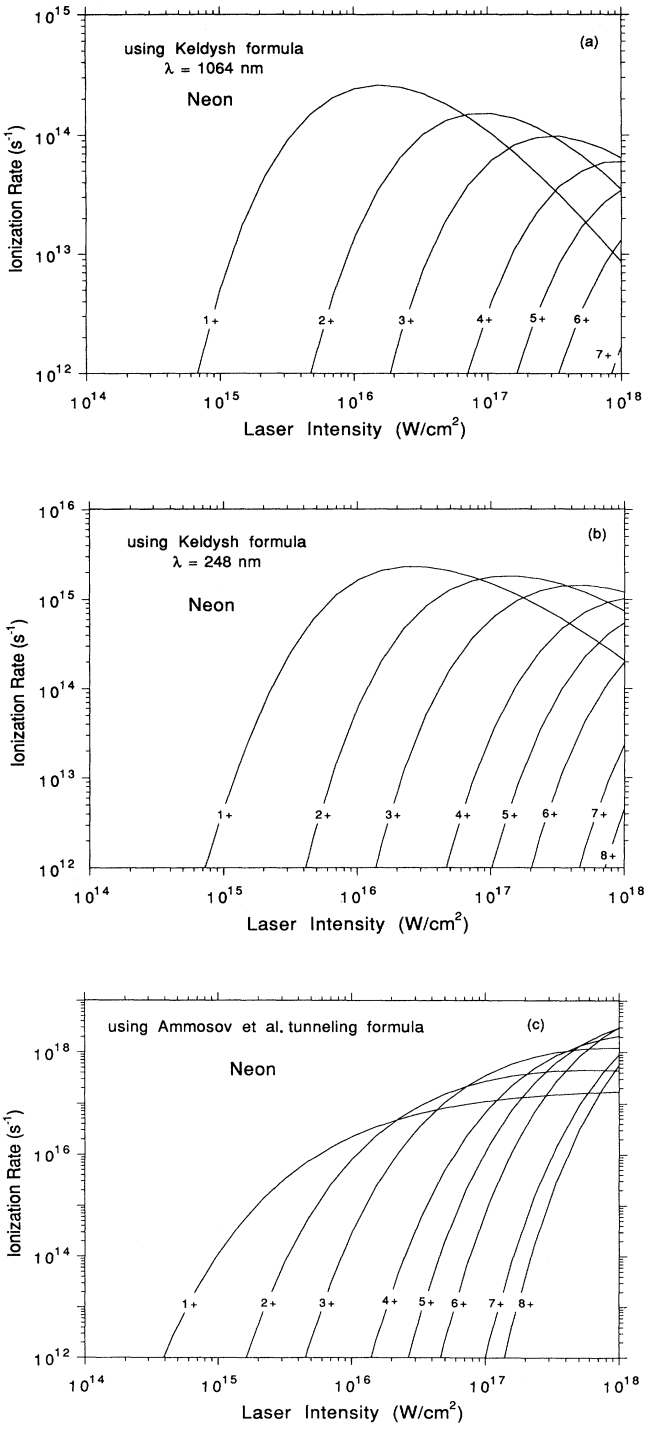

FIG. 2. Ionization rates for neon calculated using (a) full Keldysh formula [Eq. (2)] with $\lambda=1064$ nm, (b) full Keldysh formula with $\lambda=248$ nm, and (c) Ammosov *et al.* tunneling formula [Eq. (3)].

The critical laser intensity required for ionization is usually defined as that required to yield an ionization rate of 10^{12} s^{-1}. Figure 3 shows a plot of the critical laser intensity as a function of the ionization potential for the first eight charge states of neon. The Keldysh formula is in good agreement with the Coulomb-barrier model only for the first two charge states. For the higher charge states, the Ammosov *et al.* formula is in better agreement with the Coulomb-barrier model. Considering that the experiments[31,36,37] are in discord with the Keldysh theory, and in good agreement with the Ammosov *et al.* theory and the Coulomb-barrier model, we choose to do our calculations using the latter.

III. ABOVE-THRESHOLD IONIZATION

The electrons that interact with the laser are created by photoionization during the pulse. For lasers with intensities greater than 10^{16} W/cm^2 the quiver energy acquired by the electrons is much greater than the ionization potentials of the ions. For laser wavelengths of 0.25–1 μm the photon energy is much less than the ionization potentials or the quiver energy. In this case ATI can be understood from classical considerations. Burnett and Corkum[10] have shown that the excess electron energy can be attributed to the mismatch between the phase of the ionization and the crest of the electromagnetic wave. In this section we show, using this classical theory of ATI, how the residual electron energy depends on the laser parameters (such as wavelength, peak intensity, spot size, and pulse length).

Consider an electron that is created at rest at time t_0 in an electric field $E_x=E_0\sin\omega t$ (plane-polarized laser). The electron motion is given by

$$\dot{x}=\frac{eE_0}{m\omega}(\cos\omega t-\cos\omega t_0)$$

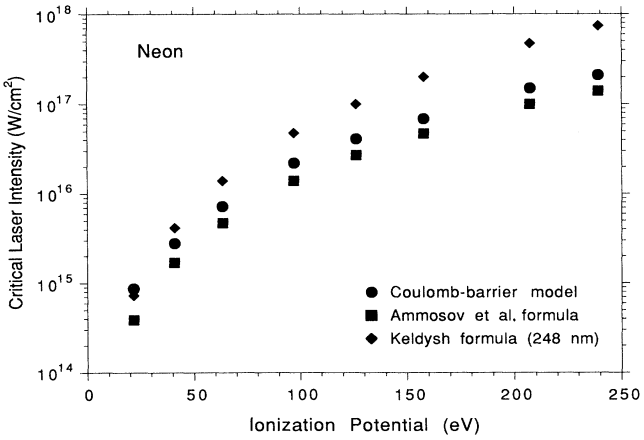

FIG. 3. Critical laser intensity required to produce the first eight charge states of neon. The required laser intensities are calculated using the Coulomb-barrier model [Eq. (1)], the Ammosov *et al.* formula [Eq. (3)], and the full Keldysh formula [Eq. (2) with $\lambda=248$ nm]. The critical laser intensity in the Ammosov *et al.* and Keldysh formulas is defined as that required to yield an ionization rate of 10^{12} s^{-1}.

and the corresponding average kinetic energy is

$$\frac{1}{2}m\langle \dot{x}^2\rangle = \frac{e^2E_0^2}{4m\omega^2}(1+2\cos^2\omega t_0) .$$

The first term in the parenthesis is the energy of the coherent oscillatory motion and the second is the energy of the direct translational motion. The second term represents the surplus electron energy, in excess of the coherent quiver energy, and is what has come to be known as the ATI energy. If the ionization occurs when $E_0\sin\omega t_0$ is maximum, i.e., when $\varphi=\omega t_0=\pi/2$, then the electron has no energy other than its quiver energy ε_q. On the other hand, an electron ionized at some arbitrary phase mismatch $\Delta\varphi$ will acquire a residual kinetic energy $\varepsilon=2\varepsilon_q\cos^2\Delta\varphi$. The average ATI energy is thus[10]

$$\langle\varepsilon\rangle=\varepsilon_q\left[\frac{2\int_0^{\pi/2}W(E(\varphi),U_i,Z)\cos^2\varphi d\varphi}{\int_0^{\pi/2}W(E(\varphi),U_i,Z)d\varphi}\right], \quad (4)$$

where $W(E(\varphi),U_i,Z)$ is the ionization rate, which is a function of the time-dependent field $E(\omega t)$, ionization potential U_i, and charge state Z.

Figure 4 shows the average ATI energy of an electron as a function of the ionization potential in neon. In Fig. 4(a) the quiver energies are 1.06×10^5, 3.20×10^4, and 5.74×10^3 eV for wavelengths of 1064, 586, and 248 nm, respectively. In Fig. 4(b) the quiver energies are 5.74×10^3, 5.74×10^2, and 5.74×10^1 eV for intensities of 10^{18}, 10^{17}, and 10^{16} W/cm^2, respectively. Note that the residual energy is larger for an electron that is released from a lower-ion-charge state. This is because when the ionization potential is small, the electron is released early in the optical cycle, and thus the phase mismatch is large. The dependence of the ATI energy on laser intensity and wavelength is strongly influenced by the dependence of the quiver energy on these parameters.

We can generalize Eq. (4) to give the average residual energy of all electrons by considering the number of electrons produced from the various charge states. Let $n_j(t)$ be the number density of charge state j at time t. The evolution of $n_j(t)$ is given by a series of first-order coupled differential equations. Assuming a stepwise ionization process,

$$\begin{aligned}\dot{n}_0(t)&=-W_1(t)n_0(t) ,\\ \dot{n}_j(t)&=W_j(t)n_{j-1}(t)-W_{j+1}(t)n_j(t) ,\\ \dot{n}_{z_{\max}}(t)&=W_{z_{\max}}(t)n_{z_{\max}-1}(t) ,\end{aligned} \quad (5)$$

where $W_j(t)$ is the ionization rate for the production of charge state j.

For a pulsed laser beam we take into account the time dependence of the field amplitude. We assume a time profile for a laser pulse in which the intensity varies as[37]

$$I(t)=I_0\mathrm{sech}^2\left[\frac{2(t-t_{\max})}{\tau_p}\right],$$

where $t_{\max}$ is the time at which the laser pulse reaches its peak value. The field is then

$$E(t)=E_0\mathrm{sech}\left[\frac{2(t-t_{\max})}{\tau_p}\right]\sin\omega t . \quad (6)$$

Since the pulse length τ_p is much greater than an optical cycle time $2\pi/\omega$, the average ATI energy is

$$\langle\varepsilon\rangle=\varepsilon_q\left[\frac{2\sum_{j=1}^{z_{\max}}\int_0^{t_{\max}}\mathrm{sech}^2\left[\frac{2(t-t_{\max})}{\tau_p}\right]n_j(t)W_j(E(t),U_i,j)\cos^2\omega t\,dt}{\sum_{j=1}^{z_{\max}}\int_0^{t_{\max}}\mathrm{sech}^2\left[\frac{2(t-t_{\max})}{\tau_p}\right]n_j(t)W_j(E(t),U_i,j)dt}\right] . \quad (7)$$

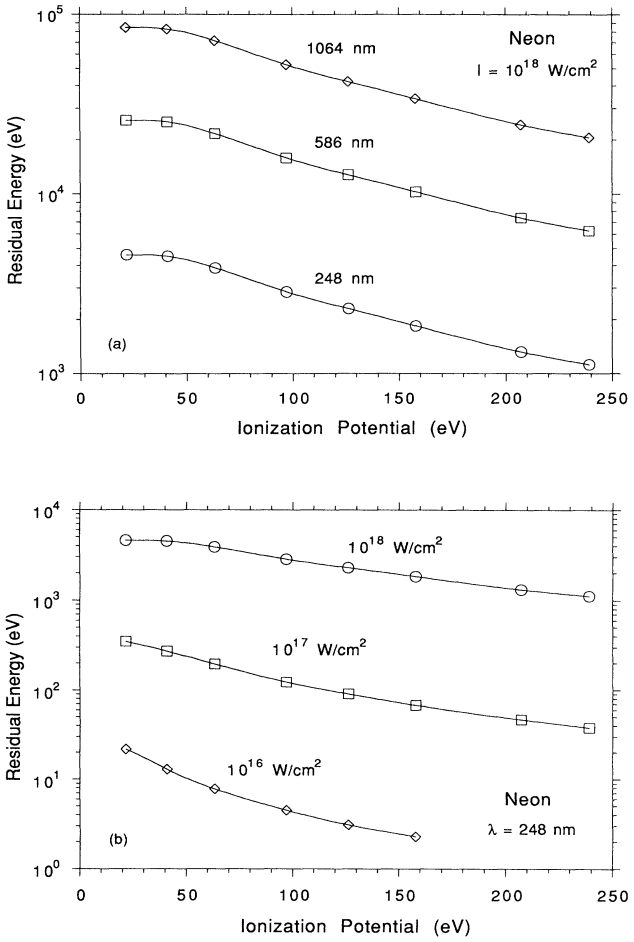

FIG. 4. Average ATI energy of a single electron [calculated using Eq. (4)] as a function of ionization potential for neon. Shown are (a) effect of laser wavelength at a peak intensity of 10^{18} W/cm^2, and (b) effect of laser peak intensity at a wavelength of 248 nm. The field varies as $E_0\sin\omega t$, where E_0 is constant. The ionization rates are calculated using Eq. (3).

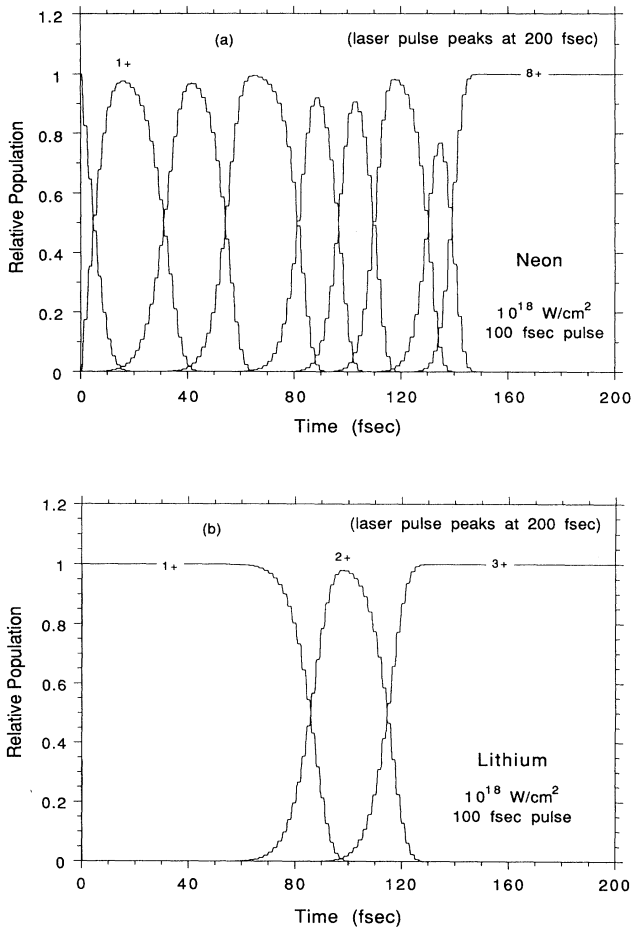

FIG. 5. Evolution of the relative population of the charge state in (a) neon and (b) lithium, for a 100-fs laser pulse with a peak intensity of 10^{18} W/cm^2. The field varies according to Eq. (6), with an optical cycle of 3.5 fs ($\lambda = 1064$ nm).

Figure 5 shows the evoluation of the charge-state populations in neon and lithium for a 100-fs laser pulse with a peak intensity of 10^{18} W/cm^2. The ionization potential for neutral neon is 21.6 eV, while that for neutral lithium is only 5.4 eV. Thus a larger number of electrons are released in lithium very early in the pulse, as compared to neon. These electrons account for the larger average ATI energy in lithium. Also note that the ATI energy for the case of a pulsed laser field is less than the ATI energy for a constant amplitude field. This is because for a pulsed field, most of the electrons from each ion charge state are released while the amplitude of the field is close to the critical field of that ion.

Figure 6 shows the residual energies in neon and lithium as a function of (a) wavelength, (b) peak intensity, and (c) pulse length. The residual energy varies with wavelength as λ^2, as expected, since the ionization rate formula used is independent of wavelength, and the dependence on wavelength comes only through the quiver energy. For neon the dependence on peak intensity goes as $I^{0.94}$, while for lithium it goes as $I^{1.04}$. This indicates that the variation of residual energy with intensity is also strongly influenced by the quiver energy. The residual energy is inversely proportional to the pulse length, but the dependence is very weak.

Consider a laser beam with a Gaussian spatial profile

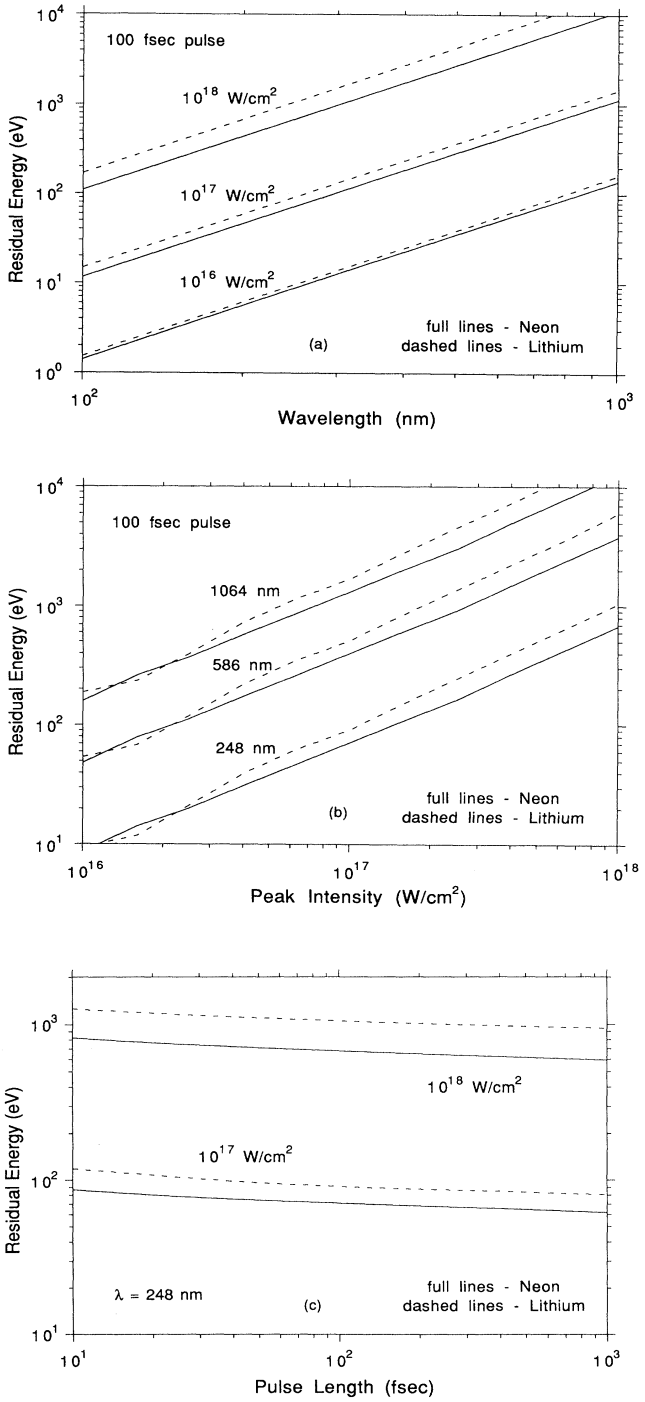

FIG. 6. Residual energy [calculated using Eq. (7)] in neon (full lines) and lithium (dashed lines) as a function of (a) wavelength, (b) peak intensity, and (c) pulse length.

$$I(r,t)=I(t)\exp(-r^2/r_0^2)$$

where r_0 is the spot size. The residual energy goes as I^n, where n is approximately 1. Performing a spatial average of the residual energy therefore gives $\frac{1}{2}$ of the values shown in Fig. 6, and independent of the spot size.

The critical laser intensity for the production of heliumlike neon and bare lithium is around 10^{17} W/cm^2 (see Fig. 1). With this peak intensity, a 100-fs laser pulse operating with a wavelength of 248 nm will produce average residual electron energies around 80 eV (Fig. 6), or around 40 eV if we take the spatial average as well. The ionization potentials for bare lithium and heliumlike neon are 122 and 239 eV, respectively. Thus the residual energies are not low enough to permit rapid recombination in these ions. In the next section we show how the presence of a space-charge field modifies the residual energy.

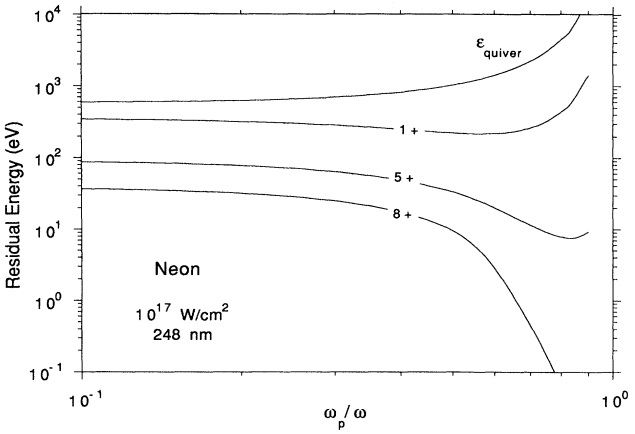

FIG. 7. Average ATI energy of a single electron [calculated using Eqs. (8) and (9)] as a function of ω_p/ω for various charge states of neon. Also shown is the modified quiver energy. The field varies as $E_0\sin\omega t$, where E_0 is constant. E_0 and ω correspond to an intensity of 10^{17} W/cm^2 and a wavelength of 248 nm, respectively.

IV. EFFECT OF SPACE CHARGE ON ABOVE-THRESHOLD IONIZATION

For high-density plasmas the motion of the electrons produces strong space-charge forces which modify the electron dynamics and the propagation of the pulse. In this section we study the generalization of the average ATI energy formulas [Eqs. (4) and (7)] for the case in which the space-charge effects are represented by a potential and the effects of the electron motion upon laser propagation are neglected. To provide a simple model for the space-charge effect, we will add a harmonic restoring force,

$$\ddot{x}+\omega_p^2 x=-\frac{eE_0}{m}\sin\omega t\ .$$

We will refer to ω_p as the plasma frequency, although its role in our calculation is only through its control of the strength of the restoring force. Consider an electron that is created at rest at $x=0$ at time t_0. The electron motion is then given by

$$\dot{x}=-\frac{eE_0}{m(\omega_p^2-\omega^2)}[\omega\cos\omega t+\cos\omega_p t(\omega\cos\omega t_0\cos\omega_p t_0+\omega_p\sin\omega t_0\sin\omega_p t_0)-\sin\omega_p t(\omega\cos\omega t_0\sin\omega_p t_0-\omega_p\sin\omega t_0\cos\omega_p t_0)]$$

and the corresponding average kinetic energy is

$$\tfrac{1}{2}m\langle\dot{x}^2\rangle=\varepsilon_q[1+2f_{\rm ex}(\omega,\omega_p,t_0)]\ ,$$

where the modified quiver energy is

$$\varepsilon_q=\frac{e^2E_0^2}{4m\omega^2}\frac{\omega^4}{(\omega_p^2-\omega^2)^2}$$

and

$$f_{\rm ex}(\omega,\omega_p,t_0)\equiv\frac{1}{2}\left[1+\frac{\sin(2\pi\omega_p/\omega)}{2\pi\omega_p/\omega}\right]\{\cos(2\omega_p t_0)[\cos^2\omega t_0-(\omega_p/\omega)^2\sin^2\omega t_0]+(\omega_p/\omega)\sin(2\omega t_0)\sin(2\omega_p t_0)\}$$
$$+\left[\frac{2}{\pi}\frac{\omega_p\omega}{(\omega_p^2-\omega^2)}\sin\left[\frac{\pi\omega_p}{\omega}\right]\right][\cos\omega t_0\cos\omega_p t_0+(\omega_p/\omega)\sin\omega t_0\sin\omega_p t_0]\ . \quad (8)$$

The function $f_{\rm ex}$ represents the excess electron energy, and is equal to $\cos^2\omega t_0$ when $\omega_p=0$. For the plasma densities and laser wavelengths of interest, $\omega_p<\omega$. What is immediately obvious is that the space-charge field is not significant in reducing the quiver energy. Any reduction in the residual energy therefore will have to come through the energy excess function $f_{\rm ex}$.

The ATI energy of a single electron in a constant amplitude field is

$$\langle\varepsilon\rangle=\varepsilon_q\left[\frac{2\int_0^{\pi/2\omega}W(E(t),U_i,Z)f_{\rm ex}(\omega,\omega_p,t)dt}{\int_0^{\pi/2\omega}W(E(t),U_i,Z)dt}\right]\ . \quad (9)$$

In this model we have assumed that the ionization rate is controlled by the applied field. Figure 7 shows the ATI energy of a single electron, coming from various charge states of neon, as a function of the ratio ω_p/ω. Also shown in Fig. 7 is the modified quiver energy. For an

electron coming from the low-ion-charge states, the reduction in excess energy due to f_{ex} is easily overwhelmed by the increase in the quiver energy. On the other hand, for the high-ion-charge states large reductions in residual energy can be achieved as the space-charge force is increased.

For a pulsed laser field, the ATI energy averaged over all charge states is

$$\langle \varepsilon \rangle = \varepsilon_q \left[\frac{2\sum_{j=1}^{z\max} \int_0^{t_{\max}} T(t) n_j(t) W_j(E(t), U_i, j) f_{ex}(\omega, \omega_p, t) dt}{\sum_{j=1}^{z\max} \int_0^{t_{\max}} T(t) n_j(t) W_j(E(t), U_i, j) dt} \right], \tag{10}$$

where $T(t)$ is the time profile of the laser intensity (sech^2 in our case). Figure 8 shows the residual energy for neon and lithium as a function of ω_p/ω for various pulse lengths. The modulation of the field amplitude has introduced an interesting effect on the excess energy. A minimum in the residual energy is achieved when

$$\omega_p \tau_{\text{pulse}} = \pi/2 \tag{11}$$

(where we have rewritten the symbol for the pulse length in order to distinguish it from the plasma period). This minimum energy is much less than the residual energy without any space-charge effect. The condition given by Eq. (11) seems to be independent of the ion species, as shown in Fig. 8. It is also independent of the peak intensity and wavelength, as shown in Fig. 9.

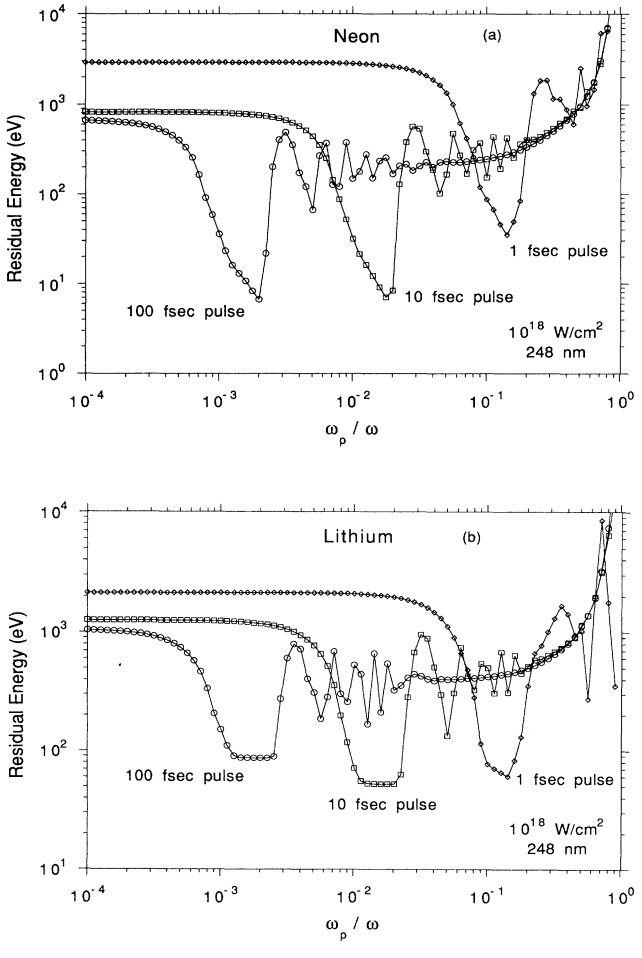

FIG. 8. Residual energy [calculated using Eqs. (8) and (10)], at various laser pulse lengths, as a function of ω_p/ω for (a) neon and (b) lithium. The peak laser intensity is 10^{18} W/cm^2 and the wavelength is 248 nm. The data points are drawn to show the resolution, in ω_p/ω, of the calculation.

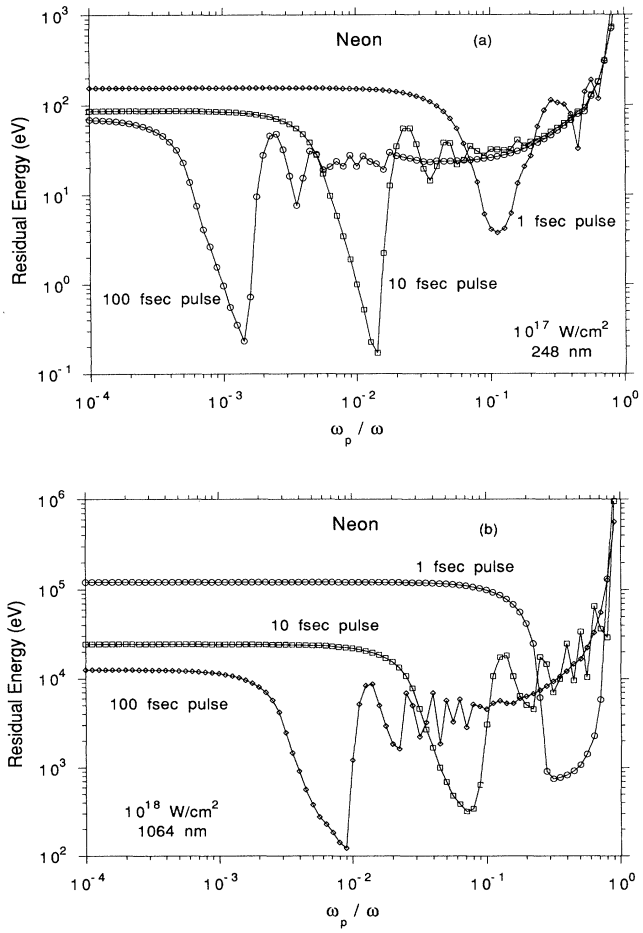

FIG. 9. Residual energy in neon, for comparison with Fig. 8(a), showing the effect of (a) peak laser intensity and (b) wavelength.

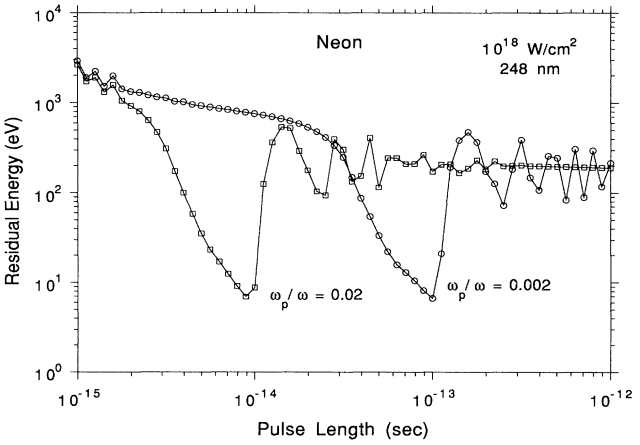

FIG. 10. Residual energy in neon [calculated using Eqs. (8) and (10)] as a function of pulse length. The peak laser intensity is 10^{18} W/cm^2 and the wavelength is 248 nm. The data points are drawn to show the resolution, in pulse length, of the calculation.

Figure 10 shows the residual energy in neon as a function of pulse length. Let us compare Fig. 10 with Fig. 6(c), which shows the residual energy as a function of pulse length in the absence of a space-charge field. Note that the residual energy obtained for a 1-ps laser pulse at an intensity of 10^{18} W/cm^2. In the absence of space-charge effects, the residual energy in neon is 600 eV. With a restoring force for which $\omega_p/\omega=0.02$, the residual energy is 200 eV. Thus even without satisfying Eq. (11), the presence of space-charge effects could significantly lower the residual energy.

In this section we have established that the presence of space-charge forces could significantly lower the residual electron energy. For a peak intensity of 10^{18} W/cm^2 (which is much beyond the critical intensity needed for the production of the neon ions we are concerned with) the residual energy can be made as low as 10 eV by properly matching the laser-pulse length to the strength of the space-charge force. In the next section we will use particle-in-cell simulations in order to provide an accurate representation of the space-charge forces which are self-consistent with the space-time profile of the plasma density and laser intensity.

V. COMPUTER SIMULATION OF SPACE-CHARGE EFFECTS

In all the calculations in this paper we deal only with the electron energies in the direction transverse to the propagation of the laser beam. This is justified because for intensities less than 10^{19} W/cm^2, the majority of the electron kinetic energy is in the transverse direction. Consider a linearly polarized plane wave described by a vector field $A_x = A_0\cos\omega t$, $A_y = A_z = 0$. In the nonrelativistic limit the two-dimensional motion of an electron that is created at rest prior to the arrival of A_0 is described by[21,22]

$$\dot{x} = -\frac{eE_0}{m\omega}\cos\omega t, \quad \dot{z} = \frac{e^2E_0^2}{2m^2c\omega^2}\cos^2\omega t \ .$$

The corresponding maximum kinetic energies are

$$\begin{aligned} \varepsilon_x &= 1.9\times10^{-13}I_0\lambda^2 \ , \\ \varepsilon_z &= 3.4\times10^{-32}I_0^2\lambda^4 \ , \end{aligned} \tag{12}$$

where I_0 is in W/cm^2, λ is in μm and the energies are in eV. Figure 11 shows the maximum transverse and longitudinal components of the kinetic energy as a function of intensity. The energies in Fig. 11 are calculated by numerically solving the relativistic Newton-Lorentz equation. For intensities below 10^{19} W/cm^2, the motion is nonrelativistic, and the solution is in excellent agreement with Eq. (12). Note that for nonrelativistic intensities the transverse kinetic energy is much larger than the longitudinal kinetic energy. In the following we will simulate the space-charge effects associated with the transverse motion of the electrons.

A self-consistent study of the effects of space-charge forces can be done through computer simulation, using a particle-in-cell (PIC) code. The particles in such codes represent swarms of electrons or ions whose motion is determined classically through the solution of

$$\ddot{x} = -\frac{e}{m}[E_a(x,t)+E_{\rm sp}(x,t)] \ ,$$

where $E_a(x,t)$ is the applied field and $E_{\rm sp}(x,t)$ is the space-charge field. The cells are partitions of configuration space. The charge density $\rho(x,t)$ in each cell is computed at each time step, and the induced electric fields are calculated from Poisson equation,

$$\frac{\partial E_{\rm sp}(x,t)}{\partial x} = 4\pi\rho(x,t) \ .$$

A very good introduction to PIC simulations is given by

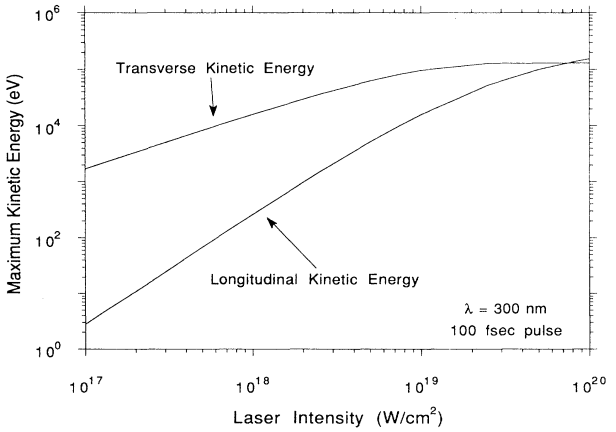

FIG. 11. The maximum transverse and longitudinal components of the kinetic energy for a single electron driven by a linearly polarized plane-wave electromagnetic field. The laser has a wavelength of 300 nm and a pulse length of 100 fs. No space-charge forces are taken into account in this figure.

Denavit and Kruer,[32] and a more complete treatment is given in Refs. 33–35.

By creating the plasma through the photoionization process described in Sec. II, we have used an ion charge-density profile that is consistent with the prescribed laser beam profile. In our simulations we take the applied field as

$$E_a(x,t)=E_0\,\mathrm{sech}\left[\frac{2(t-t_{\max})}{t_{\mathrm{pulse}}}\right]\sin\omega t\,\exp\left[-\frac{x^2}{x_0^2}\right].$$

Figure 12(a) shows the transverse profile of the ion charge density as a function of time in a neon plasma created by a XeCl laser ($\lambda=308$ nm) with a pulse length of 50 fs, peak intensity of 10^{18} W/cm^2, and spot size of 1 μm. The time coordinate in Fig. 12 goes from 0 to 200 fs, with the time arrow pointing downwards. Figure 12(b) shows a snapshot of the ion charge-density profile at the peak of the laser pulse at $t=100$ fs. One can see that the neon atoms are eight times ionized near the laser axis.

The ions move little during the passage of the pulse, but the electrons can move significantly if the space-charge forces are not too strong. Figure 13(a) shows the electron density as a function of time for an ion density of 10^{17} cm^{-3}. This figure shows the electrons being pushed away from the laser axis by the ponderomotive potential. This phenomenon has been called "electron cavitation,"[38]

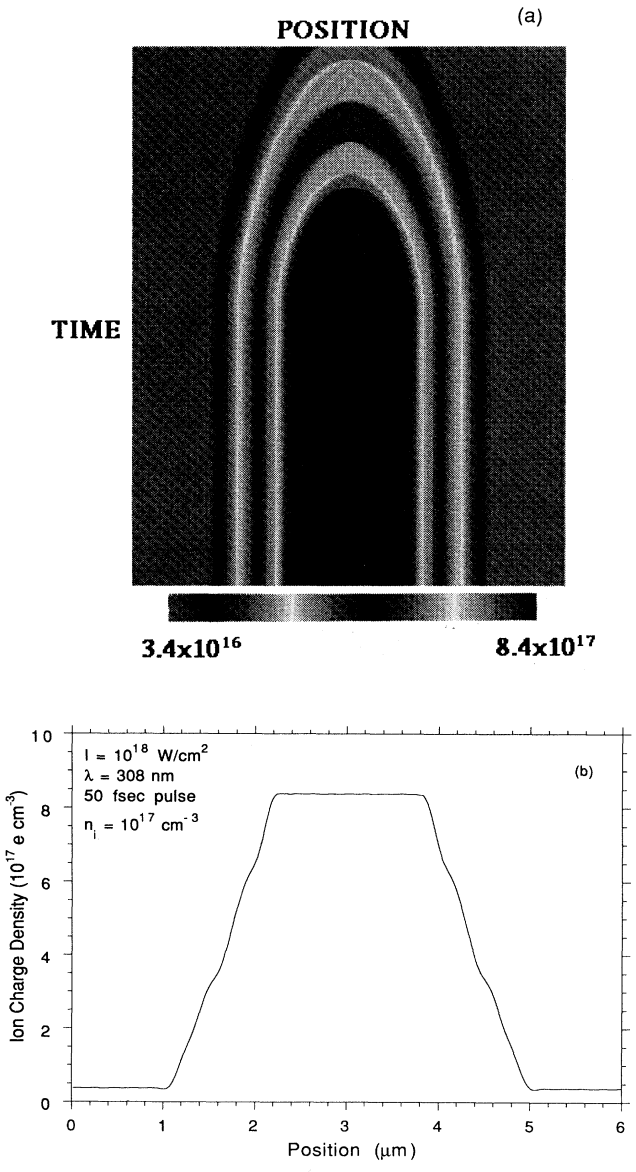

FIG. 12. Transverse profile of the ion charge density created by a linearly polarized XeCl laser pulse incident on a neon gas of density 10^{17} cm^{-3} (a) as a function of time, from $t=0$ to 200 fs (the time arrow points downwards); (b) snapshot at the peak of the laser pulse at $t=100$ fs. The laser pulse length is 50 fs, with a peak intensity of 10^{18} W/cm^2 and a spot size of 1 μm.

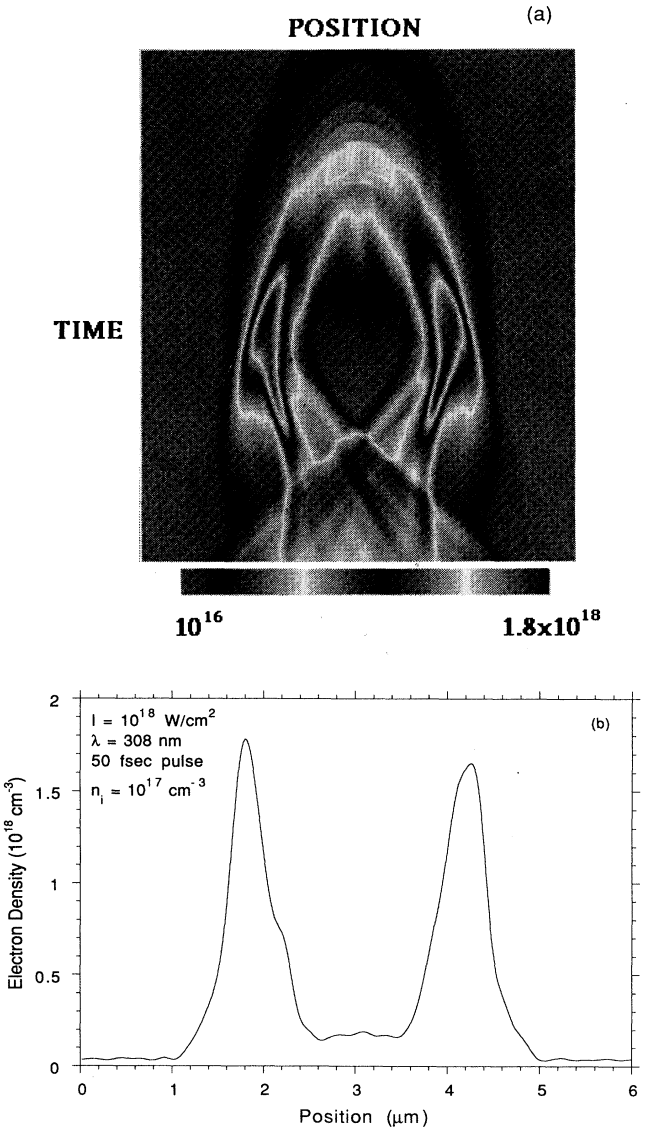

FIG. 13. Electron-density profile due to a 50-fs XeCl laser pulse of peak intensity 10^{18} W/cm^2 incident on a neon gas of density 10^{17} cm^{-3} (a) as a function of time, from $t=0$ to $=200$ fs; (b) snapshot at $t=100$ fs, showing a large electron cavitation.

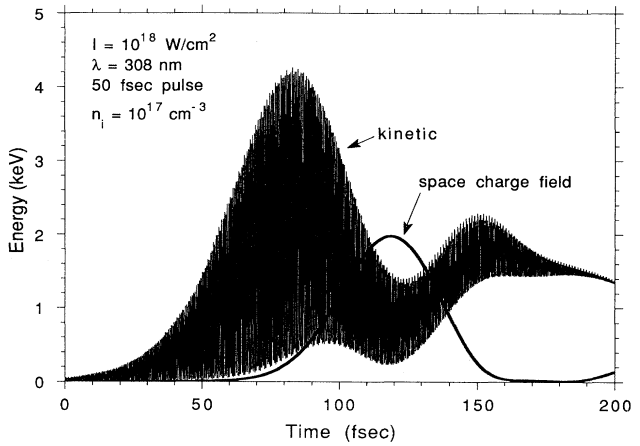

FIG. 14. History of the average kinetic and space-charge field energies in the neon plasma corresponding to Fig. 13.

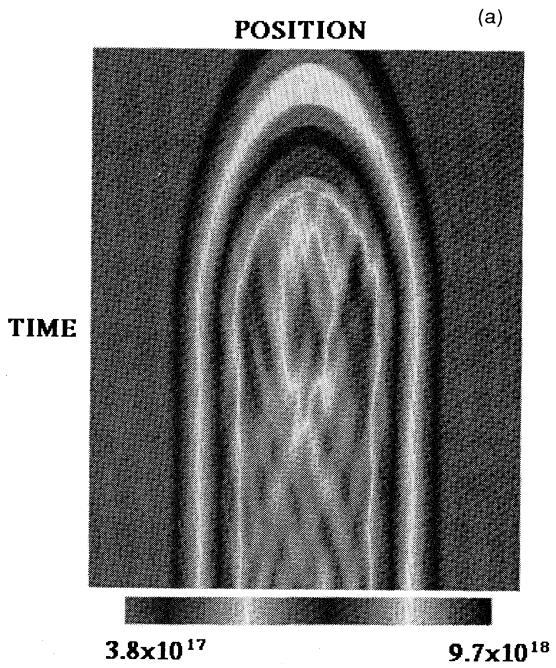

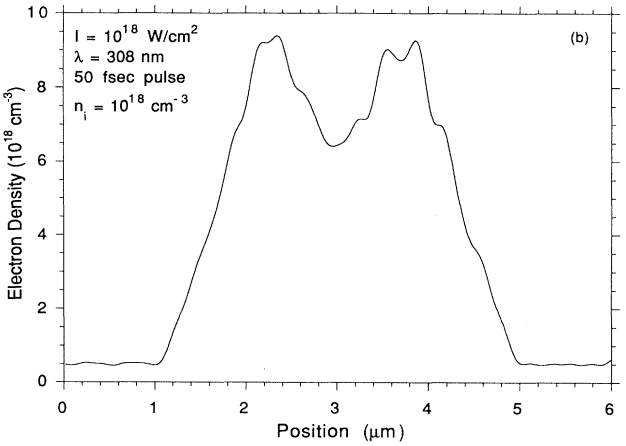

FIG. 15. Electron-density profile due to a 50-fs XeCl laser pulse of intensity 10^{18} W/cm^2 incident on a neon gas of density 10^{18} cm^{-3} (a) as a function of time, from $t=0$ to 200 fs; (b) snapshot at $t=100$ fs.

or "charge displacement."[39] Maximum cavitation happens around the peak of the laser pulse. A corresponding snapshot of the electron-density profile at the peak of the pulse is shown in Fig. 13(b). After the pulse has passed, the hole created in the plasma is filled with inrushing electrons and intense plasma oscillations are set up. This results in a large residual electron energy of about 1.4 keV. The temporal maximum of the average space-charge field energy is quite large, being of the same order of magnitude as the temporal maximum of the average electron kinetic energy, as shown in Fig. 14.

Figure 15(a) shows the history of the electron-density profile for an ion density of 10^{18} cm^{-3}. Cavitation still occurs but the cavitated channel is now very narrow compared to the size of the laser beam, as shown also in the snapshot in Fig. 15(b). The maximum space-charge field energy, shown in Fig. 16, is more than an order of magnitude less than the maximum electron kinetic energy. The residual electron energy is about 20 eV.

The cavitation effect hardly exists when the ion density is increased to 10^{19} cm^{-3}. The maximum space-charge field energy, shown in Fig. 17, is two orders of magnitude less than the maximum electron kinetic energy. The residual electron energy is still around 20 eV.

The above results show that when the plasma period is of the same order of magnitude as the laser-pulse length, large ponderomotive expulsion of the electrons occurs. This leads to large space-charge oscillations after the passage of the laser pulse, and increases the residual electron energy.

Figure 18 shows the residual electron energy in a neon plasma as a function of ion density for a 100-fs laser with a peak intensity of 10^{18} W/cm^2 at wavelengths of 1064 and 308 nm. There are two regions where the residual energy is relatively high. At the low-density end is the region where the plasma oscillation period is approximately equal to the pulse length. At the high-density end is the region where the plasma and laser frequencies are close. For XeCl lasers, residual energies as low as 20 eV can be achieved with a pulse length of 100 fs if one avoids those two resonance regions.

Figure 19 shows the dependence of the residual energy on the laser wavelength at an ion density of 10^{18} cm^{-3}. For neon the residual energy varies as $\lambda^{2.36}$, while for lithium it varies as $\lambda^{2.97}$. In the absence of space-charge effects the classical theory of ATI predicts that the dependence of the residual energy varies as λ^2, as shown in Sec. III. In the presence of a space-charge field the energy excess function [Eq. (8)] of the approximate calculation in Sec. IV predicts that the residual energy varies as λ^4. The simulations are therefore not inconsistent with the classical theory of ATI. Figure 19 confirms that short-wavelength lasers are the most suitable drivers for

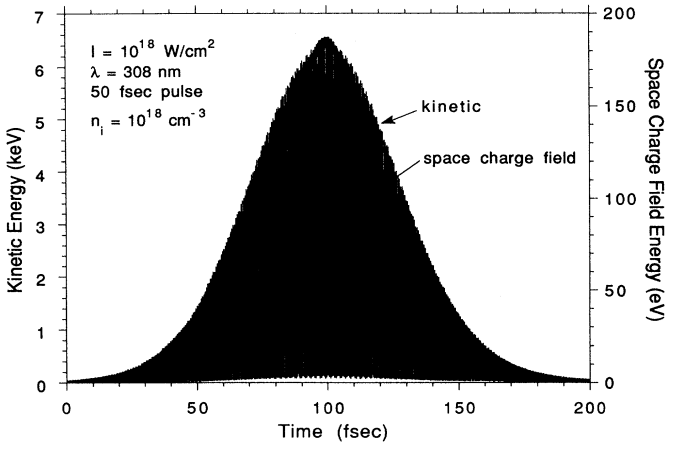

FIG. 16. History of the average kinetic and space-charge field energies in the neon plasma corresponding to Fig. 15.

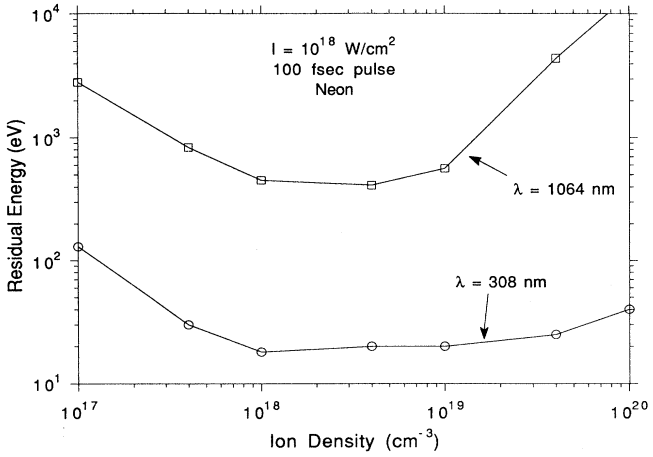

FIG. 18. Residual electron energy in a neon plasma as a function of ion density for a 100-fs laser with a peak intensity of 10^{18} W/cm^2 at wavelengths of 1064 and 308 nm.

the creation of a cold plasma.

Figure 20 shows the dependence of the residual energy on laser spot size for ion densities of 10^{17} and 10^{18} cm^{-3}. At 10^{17} cm^{-3}, space-charge oscillation due to the formation of an electron-cavitated channel is the major contributing factor to the residual energy. Since the size of the cavitation depends on the spot size of the laser beam, it follows that the residual energy in this density regime should depend strongly on the spot size. On the other hand, at 10^{18} cm^{-3}, the strong space-charge coupling between the ions and the electrons prevents the occurrence of large ponderomotive expulsion. In this case the residual energy is mainly the average ATI energy, which is independent of spot size according to the classical theory of ATI.

VI. COLLISIONAL HEATING

When the momentum of the quivering electron is changed through a collision, the coupling between the momentum and the vector potential is disturbed. This usually leads to an increase in the residual energy of the electrons and thus to the extraction of energy from the field.[22] This transfer of energy from ordered quiver motion to random motion is usually called inverse bremsstrahlung.

The inverse bremsstrahlung associated with elastic electron-ion collisions has been studied by Jones and Lee.[40] In the high-field limit the rate of transfer to thermal energy is given approximately by

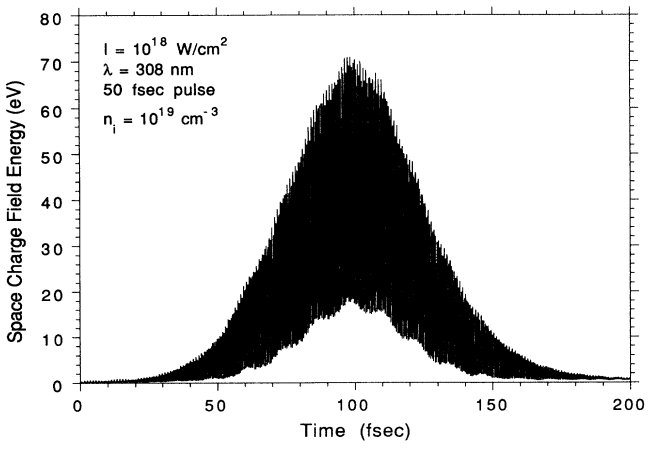

FIG. 17. History of the average space-charge field energy in the neon plasma created by a 50-fs XeCl laser pulse of peak intensity 10^{18} W/cm^2 incident on a neon gas of density 10^{19} cm^{-3}.

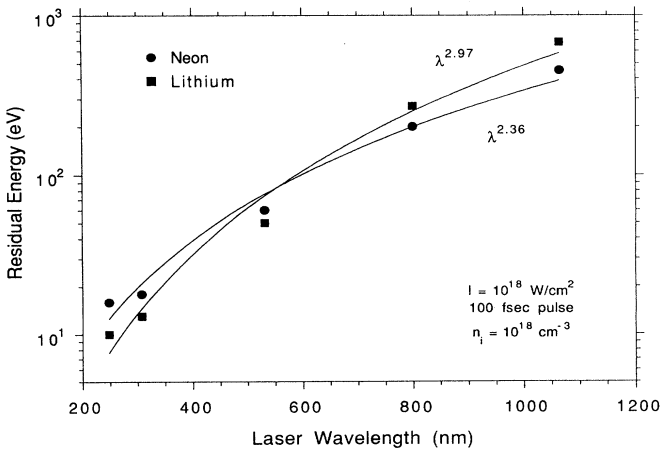

FIG. 19. Residual electron energy as a function of wavelength for a 100-fs laser with a peak intensity of 10^{18} W/cm^2. The laser is incident on a gas with a density of 10^{18} cm^{-3} The power-law fit to the simulation data is shown. For neon the residual energy varies as $\lambda^{2.36}$, while for lithium it varies as $\lambda^{2.97}$.

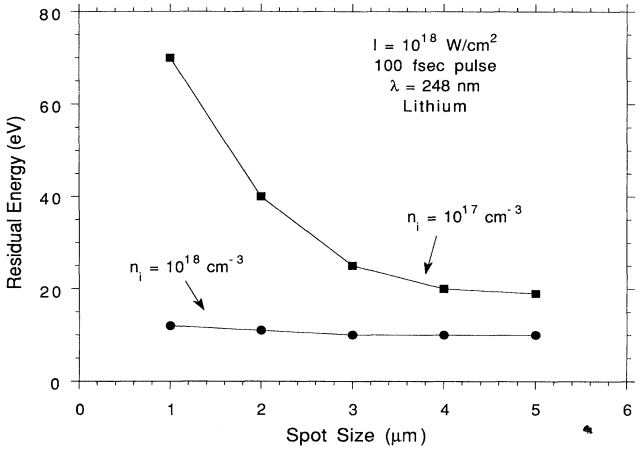

FIG. 20. Residual electron energy as a function of spot size for a 100-fs laser with a peak intensity of 10^{18} W/cm^2 and a wavelength of 248 nm. The laser is incident on a lithium gas with densities of 10^{17} and 10^{18} cm^{-3}.

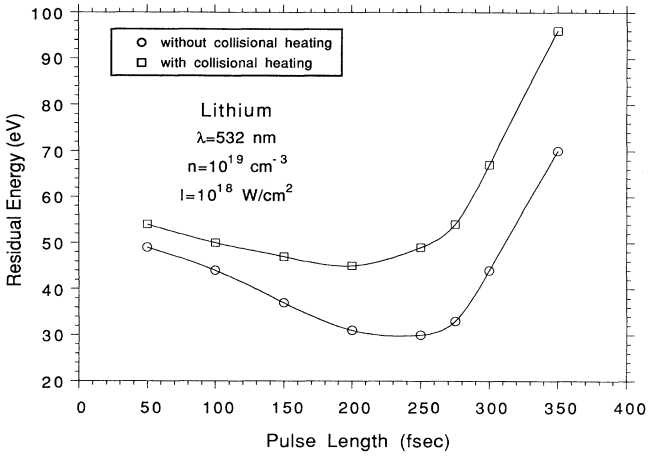

FIG. 21. Residual electron energy as a function of pulse length for a laser with a peak intensity of 10^{18} W/cm^2 and a wavelength of 532 nm. The laser is incident on a lithium gas with a density of 10^{19} cm^{-3}. Shown are the residual energies calculated with and without the contribution of collisional heating.

$$\frac{\partial}{\partial t}v_{\rm th}^2 \begin{cases} \dfrac{8}{3\pi}\dfrac{A}{v_q}\ln\left[\dfrac{mv_{\rm th}^2}{\hbar\omega}\right]\ln\left[\dfrac{v_q}{v_{\rm th}}\right] & \text{for } \begin{cases} v_q \geq v_{\rm th}\ , \\ mv_{\rm th}^2 \geq \hbar\omega\ , \end{cases} \\ 0 \quad \text{otherwise}\ , \end{cases} \tag{13}$$

where

$$A = \frac{2\pi e^4}{m^2}\sum_{i=1}^{z_{\max}} n_i Z_i^2\ .$$

In Eq. (13) $v_{\rm th}$ is the thermal speed, v_q is the quiver speed, and $\hbar\omega$ is the photon energy of the pump laser. We have incorporated Eq. (13) in our particle-in-cell code in order to provide an estimate of the conversion of quiver energy into thermal energy.

Figure 21 shows the residual energy as a function of pulse length for a 532-nm, 10^{18}-W/cm^2 laser incident on a lithium gas with a density of 10^{19} cm^{-3}. Shown in this figure are the residual energies with and without collisional heating. In the calculation with collisional heating we have assumed an initial thermal energy of 5 eV, which accounts for the difference in residual energies for a 50-fs pulse. For a 350-fs pulse, the difference in residual energies has increased to only 25 eV. The important effect shown in Fig. 21, however, is the occurrence of a minimum in the residual energy at a pulse length of 200 fs. This corresponds to the space-charge effect observed in Sec. IV. The effect of collisional heating in minimizing the residual energy is not crucial. What is important is the proper matching of the pulse length to the strength of the space-charge field.

Inelastic collisions can also lead to an increase in the residual electron energy. For example, the threshold for excitation of the Ne^{8+} ions in the center of the plasma is $\approx$920 eV. If an electron with energy just above this threshold excites a Ne^{8+} ion during the pulse, its speed will be reduced to near zero and it will be significantly out of phase with the laser field. The residual energy will be increased by an amount approximately equal to the excitation energy. However the probability of such a collision is very small. The excitation rate coefficient for e-Ne^{8+} collisions just above threshold is $\approx 2\times10^{-11}$ cm^3 s^{-1}. With an ion density of 10^{19} cm^{-3} and a total pulse length of 10^{-13} s, the probability that each electron suffers an inelastic collision of this kind is $\sim 10^{-4}$.

VII. DISCUSSION

The possibility of producing gain in plasmas that start off in ionization disequilibrium has been studied in a series of papers by Jones and Ali.[3] They do not, however, elaborate on methods for producing such a situation. The maximum population inversion that can be obtained in the transient regime depends strongly on the initial electron temperature of the recombining plasma. For electron temperatures in the range from 0.05 to 0.1 of the ionization potential (122 eV for bare lithium, 239 eV for heliumlike neon), inversion fractions from 10^{-2} to 10^{-3} are predicted from the Jones-Ali model.[3,10]

We have shown that the optimum condition for producing low residual electron energies involves ion densities around 10^{19} cm^{-3}, a pump laser with short wavelength (KrF or XeCl), and pulse lengths around 200 fs. With a peak intensity of 10^{18} W/cm^2, the residual energy in heliumlike neon plasmas, or fully stripped lithium plasmas, under this optimum condition is around 10 eV. This residual energy is just borderline for producing gain in the transient regime in these plasmas. This does not, however, preclude the use of subsidiary methods for lowering the residual energy. For example, Burnett and Corkum[10] have suggested that the average electron energy can be decreased by doping the x-ray lasing gas with a

low-ionization-potential source (such as hydrogen) in order to provide an additional source of low-ATI-energy electrons. The relatively low residual energies obtained with short-pulse laser photoionization may also facilitate the achievement of gain in the quasi-steady-state recombination phase.

ACKNOWLEDGMENTS

This work was performed under the auspices of the U.S. Department of Energy by the Lawrence Livermore National Laboratory under Contract No. W-7405-ENG-48.

[1]L. I. Gudzenko and L. A. Shelepin, Dokl. Akad. Nauk SSSR **160**, 1296 (1965) [Sov. Phys.—Dokl. **10**, 147 (1965)].

[2]J. Peyraud and N. Peyraud, J. Appl. Phys. **43**, 2993 (1972).

[3]W. W. Jones and A. W. Ali, Appl. Phys. Lett. **26**, 450 (1975); J. Appl. Phys. **48**, 3118 (1977); J. Phys. B **11**, 187 (1978).

[4]J. M. Green and W. T. Silfvast, Appl. Phys. Lett. **28**, 253 (1976).

[5]G. J. Pert, J. Phys. B **9**, 3301 (1976).

[6]G. J. Tallents, J. Phys. B **10**, 1769 (1977).

[7]S. Suckewer and H. Fishman, J. Appl. Phys. **51**, 1922 (1979); S. Suckewer, C. H. Skinner, M. Milchberg, C. Keane, and D. Voorhees, Phys. Rev. Lett. **55**, 1753 (1985).

[8]C. Chenais-Popovics, R. Corbett, J. Hooker, M. H. Key, G. P. Kiehn, C. L. S. Lewis, G. J. Pert, C. Regan, S. J. Rose, S. Sadaat, R. Smith, T. Tomie, and O. Willi, Phys. Rev. Lett. **59**, 2161 (1987); C. L. S. Lewis, R. Corbett, D. O'Neill, C. Regan, S. Sadaat, C. Chenais-Popovics, T. Tomie, J. Edwards, G. P. Kiehn, R. Smith, O. Willi, A. Carillon, H. Guennou, P. Jaegle, G. Jamelot, A. Klisnick, A. Sureau, M. Grande, C. Hooker, M. H. Key, S. J. Rose, I. N. Ross, P. T. Rumsby, G. J. Pert, and S. A. Ramsden, Plasma Phys. Controlled Fusion **30**, 35 (1988).

[9]P. Jaegle, G. Jamelot, A. Carillon, A. Klisnick, A. Sureau, and H. Guennou, J. Opt. Soc. Am. B **4**, 563 (1987).

[10]N. H. Burnett and P. B. Corkum, J. Opt. Soc. Am. B **6**, 1195 (1989); N. H. Burnett and G. D. Enright, IEEE J. Quantum Electron. **QE-26**, 1797 (1990).

[11]T. S. Luk, T. Graber, H. Jara, U. Johann, K. Boyer, and C. K. Rhodes, J. Opt. Soc. Am. B **4**, 847 (1987); A. McPherson, G. Gibson, H. Jara, V. Johann, T. S. Luk, I. A. McIntyre, K. Boyer, and C. K. Rhodes, *ibid.* **4**, 595 (1987); T. S. Luk, K. Boyer, A. McPherson, G. Gibson, X. Shi, and C. K. Rhodes, Opt. Soc. Am. Tech. Digest **17**, 43 (1989).

[12]J. P. Roberts, A. J. Taylor, P. H. Y. Lee, and R. B. Gibson, Opt. Lett. **13**, 734 (1988); J. A. Cobble, G. A. Kyrala, A. A. Hauer, A. J. Taylor, C. C. Gomes, N. D. Delameter, and G. T. Schappert, Phys. Rev. A **39**, 454 (1989); P. H. Y. Lee, D. E. Casperson, and G. T. Schappert, Phys. Rev. A **40**, 1363 (1989); G. T. Schappert, D. E. Casperson, J. A. Cobble, L. A. Jones, G. A. Kyrala, P.H. Y. Lee, T. D. Nichols, A. J. Taylor, and C. R. Tallman, Opt. Soc. Am. Tech. Digest **17**, 35 (1989).

[13]M. M. Murnane, H. C. Kapteyn, and R. W. Falcone, Phys. Rev. Lett. **62**, 155 (1989).

[14]C. H. Nam, W. Tighe, S. Suckewer, J. F. Seely, V. Feldman, and L. A. Woltz, Phys. Rev. Lett. **59**, 2427 (1987); S. Suckewer, Opt. Soc. Am. Tech. Digest **17**, 44 (1989).

[15]P. Maine, D. Strickland, P. Bado, M. Pessot, and G. Mouron, IEEE J. Quantum Electron. **24**, 398 (1988).

[16]D. Kuhlke, U. Herpers, and D. von der Linde, Appl. Phys. Lett. **50**, 1785 (1987).

[17]J. R. M. Barr, N. J. Everall, C. J. Hooker, I. N. Ross, M. J. Shaw, and W. T. Toner, Opt. Commun. **60**, 127 (1988); O. Willi, G. Kiehn, J. Edwards, V. Barrow, and R. Smith, Opt. Soc. Am. Tech. Digest **17**, 30 (1989).

[18]W. M. Wood, G. Focht, and M. C. Downer, Opt. Lett. **13**, 984 (1988).

[19]H. Shiraga, K. Yamakawa, C. P. J. Barty, M. Nishio, and Y. Kato, Opt. Soc. Am. Tech. Digest **17**, 26 (1989).

[20]M. D. Perry, F. G. Patterson, J. Weston, and E. M. Campbell, Opt. Soc. Am. Tech. Digest **17**, 39 (1989).

[21]E. S. Sarachik and G. T. Schappert, Phys. Rev. D **1**, 2738 (1970).

[22]J. N. Bardsley, B. M. Penetrante, and M. H. Mittleman, Phys. Rev. A **40**, 3823 (1989).

[23]P. Agostini, F. Fabre, G. Mainfray, G. Petite, and N. K. Rahman, Phys. Rev. Lett. **42**, 1127 (1979).

[24]R. R. Freeman, P. H. Bucksbaum, M. Milchberg, S. Darack, D. Schumacher, and M. E. Geusic, Phys. Rev. Lett. **59**, 1092 (1987).

[25]T. F. Gallagher, Phys. Rev. Lett. **61**, 2304 (1988).

[26]P. B. Corkum, N. H. Burnett, and F. Brunel, Phys. Rev. Lett. **62**, 1259 (1989).

[27]L. V. Keldysh, Zh. Eksp. Teor. Fiz. **47**, 1945 (1964) [Sov. Phys.—JETP **20**, 1307 (1965)].

[28]A. M. Perelomov, V. S. Popov, and M. V. Terentev, Zh. Eksp. Teor. Fiz. **50**, 1393 (1966) [Sov. Phys.—JETP **23**, 924 (1965)].

[29]L. D. Landau and E. M. Lifshitz, *Quantum Mechanics,* 3rd ed. (Pergamon, London, 1978).

[30]M. V. Ammosov, N. B. Delone, and V. P. Krainov, Zh. Eksp. Teor. Fiz. **91**, 2008 (1986) [Sov. Phys.—JETP **64**, 1191 (1986)].

[31]S. Augst, D. Strickland, D. D. Meyerhofer, S. L. Chin, and J. H. Eberly, Phys. Rev. Lett. **63**, 2212 (1989).

[32]J. Denavit and W. L. Kruer, Comments Plasma Phys. Controlled Fusion **6**, 35 (1980); W. L. Kruer, *The Physics of Laser Plasma Interactions* (Addison-Wesley, New York, 1988).

[33]C. K. Birdsall and A. B. Langdon, *Plasma Physics via Computer Simulation* (McGraw-Hill, New York, 1985).

[34]R. W. Hockney and J. W. Eastwood, *Computer Simulation Using Particles* (McGraw-Hill, New York, 1981).

[35]T. Tajima, *Computational Plasma Physics: With Applications to Fusion and Astrophysics* (Addison-Wesley, New York, 1989).

[36]S. L. Chin, F. Yergeau, and P. Lavigne, J. Phys. B **18**, L213 (1985); F. Yergeau, S. L. Chin, and P. Lavigne, J. Phys. B **20**, 723 (1987).

[37]M. D. Perry, O. L. Landen, A. Szoke, and E. M. Campbell, Phys. Rev. A **37**, 747 (1988).

[38]G. Z. Sun, E. Ott, Y. C. Lee, and P. Guzdar, Phys. Fluids **30**, 526 (1987).

[39]J. C. Solem, T. S. Luk, K. Boyer, and C. K. Rhodes, IEEE J. Quantum Electron. **25**, 2423 (1989).

[40]R. D. Jones and K. Lee, Phys. Fluids **25**, 2307 (1982).

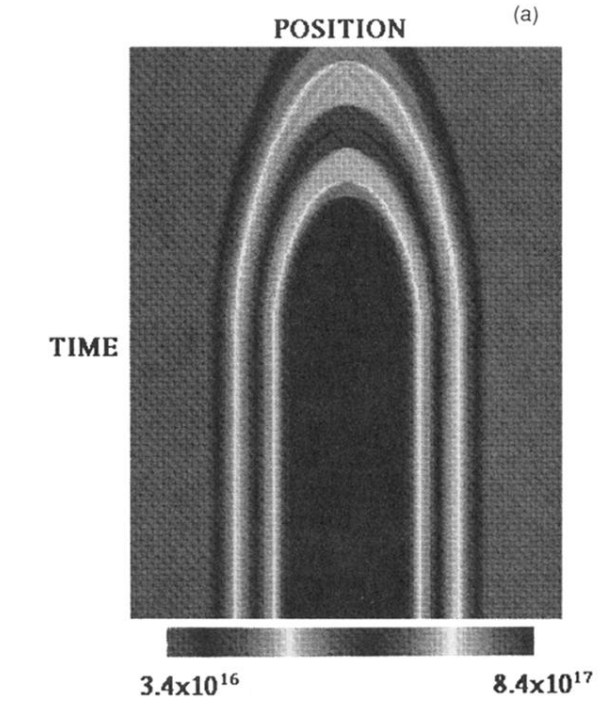

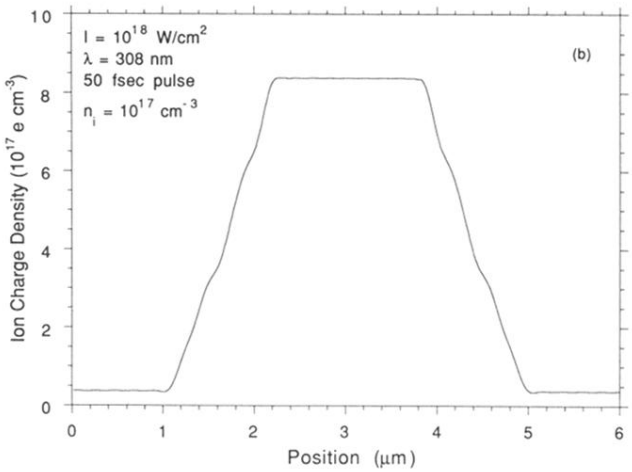

FIG. 12. Transverse profile of the ion charge density created by a linearly polarized XeCl laser pulse incident on a neon gas of density 10^{17} cm^{-3} (a) as a function of time, from $t=0$ to 200 fs (the time arrow points downwards); (b) snapshot at the peak of the laser pulse at $t=100$ fs. The laser pulse length is 50 fs, with a peak intensity of 10^{18} W/cm^2 and a spot size of 1 μm.

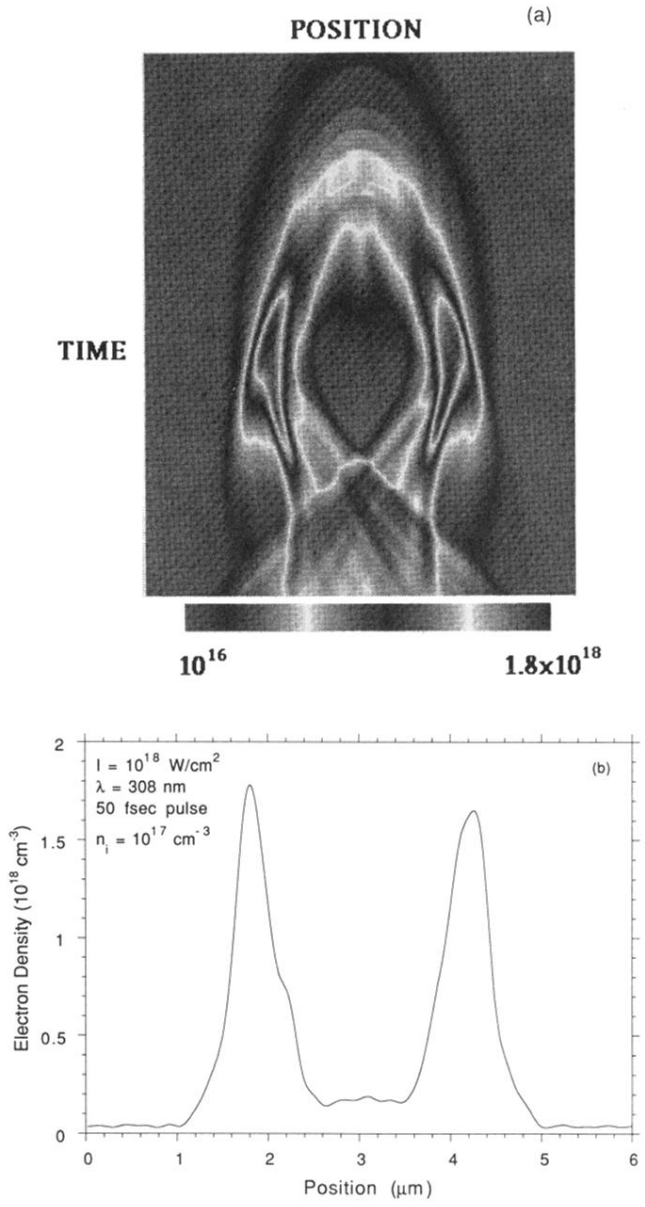

FIG. 13. Electron-density profile due to a 50-fs XeCl laser pulse of peak intensity 10^{18} W/cm^2 incident on a neon gas of density 10^{17} cm^{-3} (a) as a function of time, from $t=0$ to $=200$ fs; (b) snapshot at $t=100$ fs, showing a large electron cavitation.

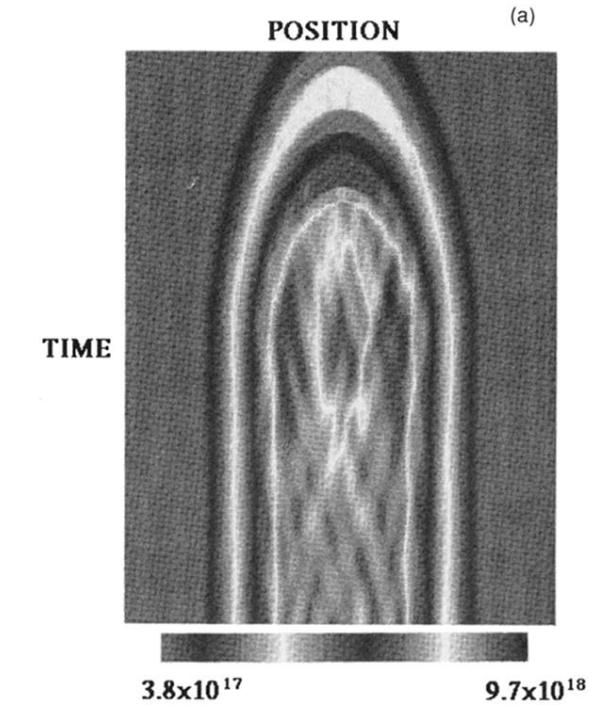

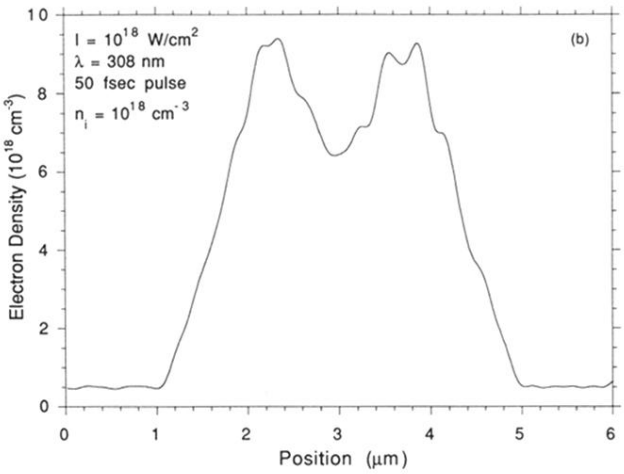

FIG. 15. Electron-density profile due to a 50-fs XeCl laser pulse of intensity 10^{18} W/cm^2 incident on a neon gas of density 10^{18} cm^{-3} (a) as a function of time, from $t=0$ to 200 fs; (b) snapshot at $t=100$ fs.